基礎研究

# 超低充填小児ECMOシステムの開発と基礎研究

林　輝行*，巽　英介*2，片桐伸将*2，水野敏秀*2，吉田幸太郎*，八木原俊克*3

## Ⅰ．緒　言

今日，重篤な急性呼吸循環不全症例において経皮的心肺補助法PCPS（percutaneous cardiopulmonary support）は極めて重要な救命補助手段として広く認知されている。一方で従来の呼吸管理では救命不可能な急性の重症呼吸不全患者においては，ECMO（extracorporeal membrane oxygenation）が唯一の救命補助手段となる。米国ELSO（Extracorporeal Life Support Organization）registry report 2004[1]によると，1986年より登録されたECMO症例28,985例のうち27,407例（94.6％）が新生児または小児症例である。このうち呼吸補助を目的として導入された21,823例の離脱率は74.3％と確固とした治療手段として定着しているのに対して，急性心肺蘇生および循環不全症例に対する離脱率は40.7％（2,273/5,584例）と未だ満足のいく治療成績ではない。現在，国立循環器病センターにおける小児補助循環システムは，早期の循環回復を目的とした迅速導入用超低充填補助循環システムと比較的抗血栓性に優れた中期使用可能な補助循環システムによる段階的導入法を採用している[2]。迅速導入が可能な小児補助循環システムとして，平和物産社製BIO-99®を使用している（図1）。この現行システ

Key word
ECMO
neonate
infant
cardiopulmonary resuscitation
heparin coating

Development and *in vivo* Testing of an Ultra-Compact Extracorporeal Membrane Oxygenation (ECMO) System for Pediatric Use

*Teruyuki Hayashi, Kotaro Yoshida :
Department of Clinical Engineer,
National Cardiovascular Center
国立循環器病センター 臨床工学
*2Eisuke Tatsumi, Nobumasa Katagiri,
Toshihide Mizuno :
Department of Artificial Organs,
Advanced Medical Engineering Center,
National Cardiovascular Center Research Institute
国立循環器病センター研究所
先進医工学センター 人工臓器部
*3Toshikatu Yagihara :
Deputy Director General of the Hospital,
National Cardiovascular Center
国立循環器病センター 副院長

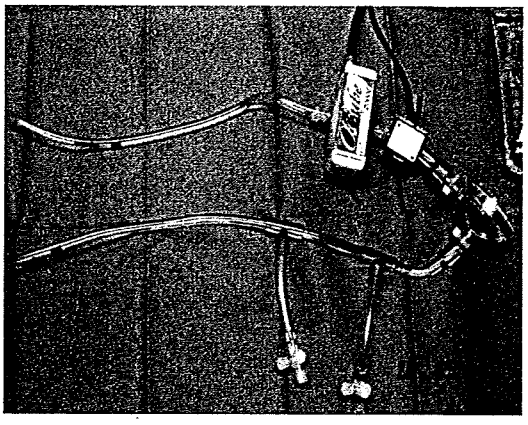

図1．迅速導入用超低充填小児補助循環システム
平和物産社製BIO-99®

ムは，循環血液量の少ない新生児・小児に対して血液希釈の影響を最小限にするために，充填量の最少化を最優先したシステムである。総充填量は99mLで，体重2.5kgの新生児においても無輸血充填が可能であり，急性心肺不全が発生しても迅速な対応が可能である。しかし問題点として，①充填量削減を最優先するために熱交換器を内蔵しない人工肺を採用しており，導入開始直後より体温調節機能の未発達な新生児では，体温低下を併発する，②ヘパリンコーティング化された人工肺を採用しているが，遠心ポンプと回路はヘパリンコーティング化されておらず，抗血栓性について不安が残る，③開発当時はプレコネクト化されたシステムであったが，現在は人工肺が別包されて回路との接続が必要となりセットアップに時間を要する，などが残されていた。このような現行システムの抱える問題点を改善した新規迅速導入用超低充填小児補助循環システムを構成するために，デバイス選定と臨床導入前基礎研究を行い，新規システムの評価を行った。

## Ⅱ．方　法

### 1．新規システムのデバイス選択

新規システムの人工肺として，JMS社製OXIA IC®を採用した。この人工肺は熱交換器内蔵型でありながら，充填量は37mLと現行システムの人工肺より充填量は少ない。人工肺の膜素材としてポリプロピレン中空糸膜を採用しており，熱交換器を含めた全ての血液接触面にはJMS社独自のヘパリンコーティングCOAFREE®，COAFREE® Ⅱが採用されている[3]。遠心ポンプには，現在市販されているもので最も充填量が少ないJMS社製遠心ポンプMIX FLOW 3®を新デバイスとして採用した。充填量は18mLで，人工肺同様全ての血液接触面にはヘパリンコーティングCOAFREE® Ⅱが採用されている。これらをCOAFREE®ヘパリンコーティングが施されたポリ塩化ビニル（PVC）チューブでプレコネクト化した新規迅速導入用超低充填小児補助循環システムを作成した。現行システムからの主な改善点として，体温調節を可能とする熱交換器内蔵型人工肺の採用，抗血栓性の向上を目指して新規システムの全血液接触面に対するヘパリンコーティング化，さらに迅速なセットアップを可能とするプレコネクト化を実現した。今回の実験モデルの充填量は110mLであるが，臨床導入予定新規システムの充填量は90mLを予定しており，現行システムと比較して熱交換器内蔵型でありながら低充填化を可能とした（図2）。

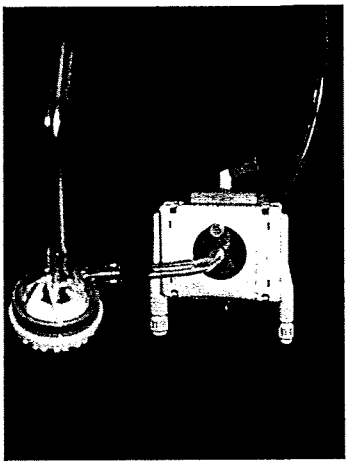

| | |
|---|---|
| priming volume | 90mL |
| heat exchanger | + |
| heparin coating | + |
| pre-connecting | + |
| max blood Flow | 2.0L/min |

図2．新規迅速導入用超低充填小児補助循環システム

### 2．新規システムの*in vivo*評価

安全性，抗血栓性，およびガス交換能の検討を目的に*in vivo*評価を行った。新規シス

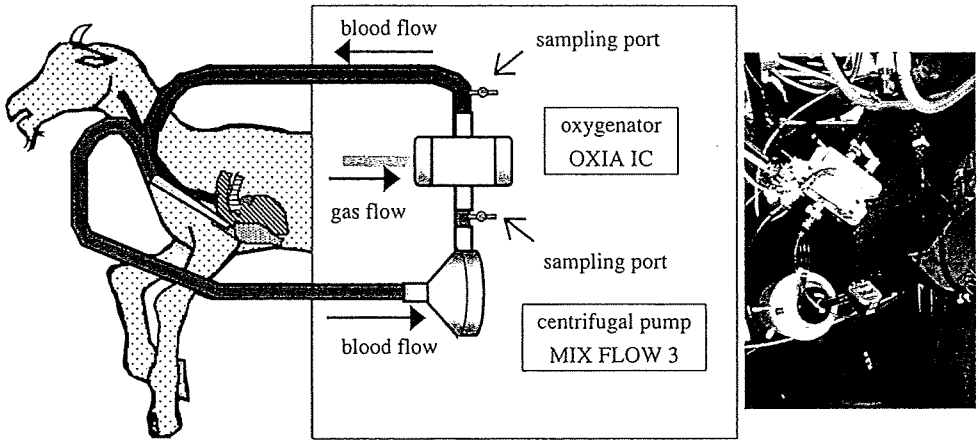


図3．補助循環システムの実験シェーマと実験風景

テムを使用して，体重17kgと21kgの成シバ山羊2頭で，24時間の急性動物実験を行った[4]。右心房脱血，頸動脈送血にて静-動脈バイパス回路を作成した(図3)。イソフルランとケタミンによる麻酔導入後，気管内挿管を行い全身麻酔下で左大腿動脈から動脈圧ライン，左外頸静脈より中心静脈圧(CVP)および薬液注入用のダブルルーメンカテーテルラインを挿入した。抗凝固剤として，ヘパリンナトリウム(ヘパリン®)100IU/kgを送脱血管挿入時に投与した。右内頸静脈よりメドトロニック社製Bio-Medicus® Venous cannula 17Fr，右内頸動脈より同社製Bio-Medicus® Arterial cannula 15Frを挿入し，新規補助循環システムの運転を開始した。ACTが150～200秒になるようにヘパリンナトリウムの持続投与を行い，24時間の連続灌流を実施した。血液流量は超音波ドップラー血流計(Transonic, USA)にて1.5±0.5L/minとなるように適宜回転数を調節した。なお，本研究の動物実験にあたっては，国立循環器病センター実験動物福祉小委員会の規程を遵守した。

### 3．測定スケジュールと評価項目

灌流開始前，灌流開始後1，2，3，6，12，18，24時間において，下記評価項目の測定を行った。人工肺，遠心ポンプの評価を目的として，人工肺圧力損失，灌流量，遠心ポンプ回転数を記録した。人工肺のガス交換能については，以下の計算式を用いて，人工肺酸素移動量($\dot{V}O_2$)および炭酸ガス移動量($\dot{V}CO_2$)を算出した。

$$\dot{V}O_2 = \{(SaO_2 - SvO_2)/100 \times 1.34 \times Hb + 0.003 \times (PaO_2 - PvO_2)\} \times Qb/100$$

$$\dot{V}CO_2 = 2.226 \times (tvCO_2 - taCO_2)/100 \times Qb$$

$SaO_2$：人工肺流出側血液酸素飽和度(%)
$SvO_2$：人工肺流入側血液酸素飽和度(%)
$PaO_2$：人工肺血液流出側酸素分圧(mmHg)
$PvO_2$：人工肺血液流入側酸素分圧(mmHg)
Hb　：血液ヘモグロビン濃度(g/dL)
Qb　：血液流量(mL/min)
1.34　：ヘモグロビン酸素容量(mL/g)
0.003：37℃血液への酸素溶解度(vol%/mmHg)
$tvCO_2$：人工肺血液流入側炭酸ガス含量(mmol/L)
$taCO_2$：人工肺血液流出側炭酸ガス含量

(mmol/L)

2.226：mmol/Lからmg/dLへの変換係数

吹送ガス流量/血液流量比1.0，酸素濃度100％において人工肺の流入部および流出部で血液を採取し，血液ガス分析装置(ABL-500 and OSM-3, Radiometer, Copenhagen Denmark)を用いて血液ガス値を計測した。血液成分の変化として，血中ヘモグロビン濃度，血小板数を測定した。凝固機能検査として，賦活化血液凝固時間(ACT)，活性化部分トロンボプラスチン時間(APTT)，血清ヘパリン濃度，アンチトロンビンⅢ(ATⅢ)を測定した。実験終了後は人工肺，遠心ポンプ，血液回路，送脱血管等のシステム血液接触面について肉眼的に血栓の分布状態を観察した。

## Ⅲ. 結　果

人工肺および遠心ポンプの機能低下は，2例ともに認めなかった。人工肺圧力損失は30～50mmHgと低値で経過し，遠心ポンプの回転数は3,000～4,000RPM，血液流量は1.2～1.5L/minと安定した状態で実験予定期間を終了することが可能であった(図4)。2例ともに実験を通してガス交換能は良好に保たれており，$\dot{V}O_2$は平均55.2mL/min (Case 1)，61.6mL/min (Case 2)，$\dot{V}CO_2$は平均59.7mL/min (Case 1)，61.4mL/min (Case 2)で経過した(図5)。人工肺からの血漿リークも，一切観察されなかった。血液成分の変化に関しては，血中ヘモグロビン濃度と血小板数は開始後3時間までの血液希釈による影響を除けば，著変なく経過した(図6)。ACTは，実験開始後3時間までの送脱血管挿入時のヘパリ

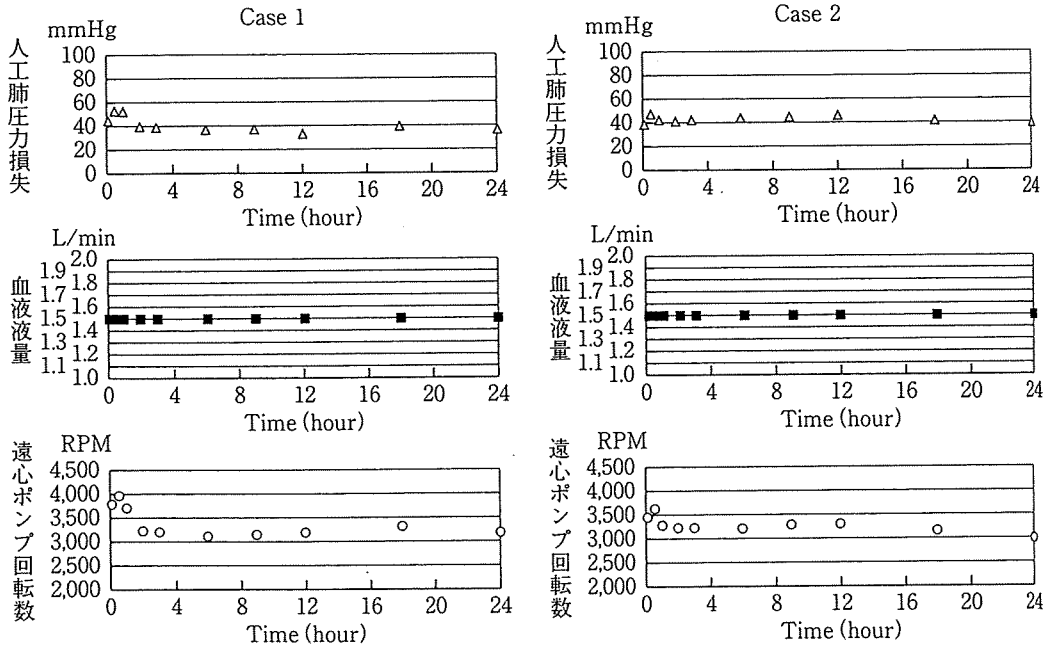


図4. 人工肺圧力損失・血液流量・遠心ポンプ回転数

ンナトリウム投与の影響による延長を除けば，150～200秒に調節が可能であった。APTTは，Case 1で2時間後に最大値300秒となったが，その後は低下した(図7)。終了後のシステムの肉眼的観察において，遠心ポンプのピボット部に少量の血栓付着を認めた。人工肺は，熱交換器流入部，血液流出部に血栓形成を認めず，分解後の熱交換部分，人工肺中空糸部分の評価においても，血栓は観察されなかった(図8)。

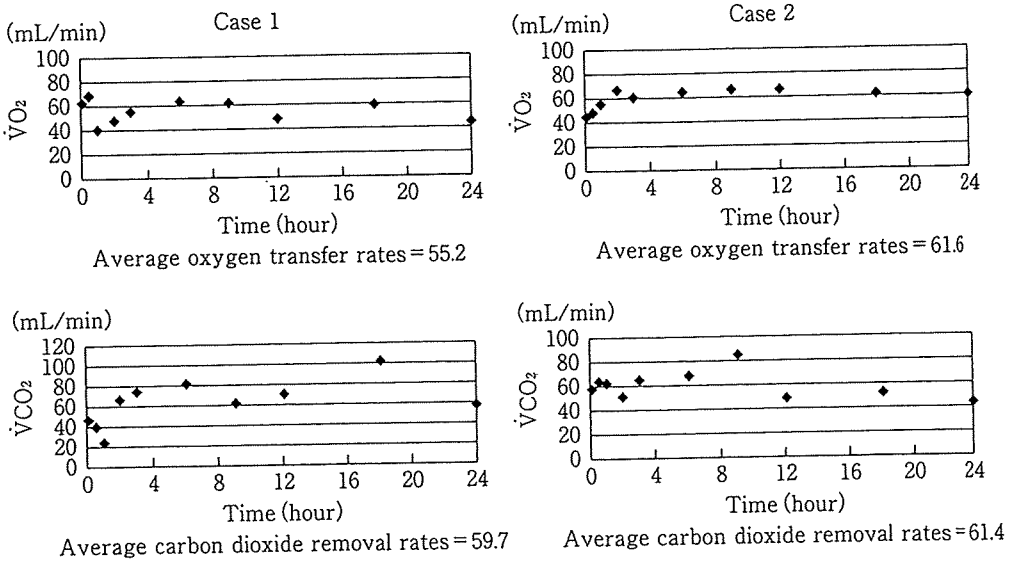


図5. $\dot{V}O_2$・$\dot{V}CO_2$

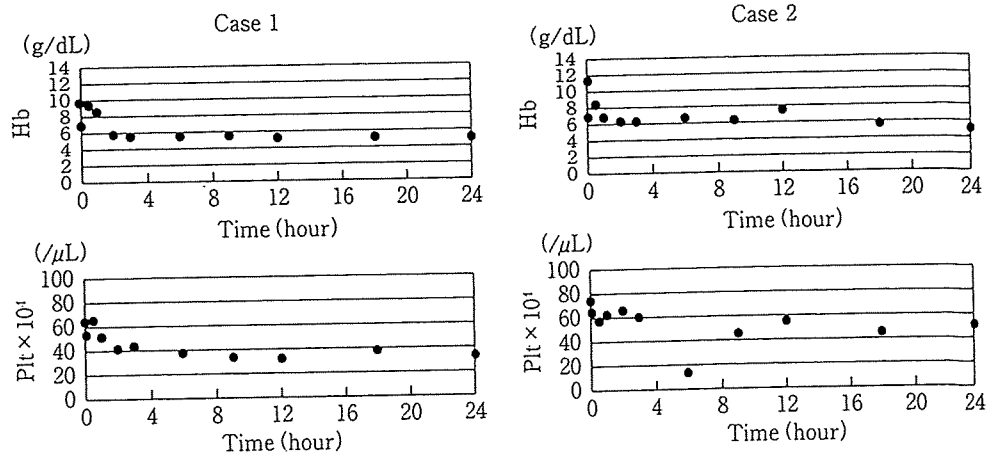


図6. ヘモグロビン濃度・血小板数

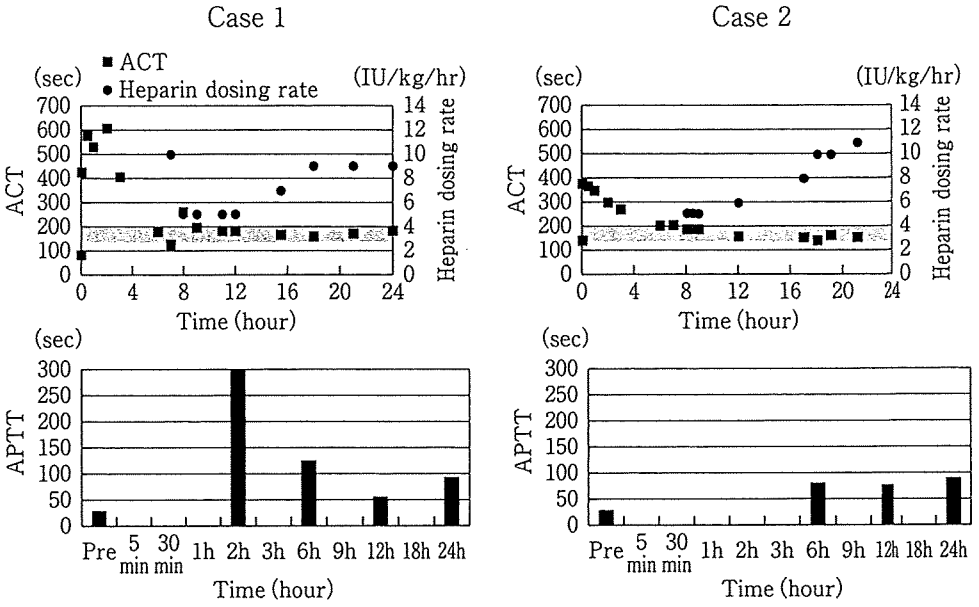


図7. ACT・ヘパリンナトリウム投与量・APTT

## Ⅳ. 考　察

新生児・小児領域の循環補助の適応は，急性心室機能不全をはじめ，高度低酸素血症や種々のショックなど広範囲に及び，緊急度の高い場合も多く，迅速なセットアップが要求される[5,6]。従って基本回路構成を単純化し，組み立てや充填に要する時間をできる限り短縮する工夫が必須である。このような背景を踏まえて，国立循環器病センターにおける小児補助循環システムは，2000年1月より，早期の循環回復を目的とした迅速導入用補助循環システムと，比較的抗血栓性に優れた中期使用可能な補助循環システムの2種類のシステムを段階的に使用する手法を採用している[7]。迅速導入用補助循環システムは，循環血液量の少ない新生児・小児に対して血液希釈の影響を最小限にするために，充填量最少化を優先したシステムである。総充填量は99mLで，体重2.5kgの新生児においても無輸血充填と迅速導入が可能である。しかし，充填量削減を最優先するために熱交換器を内蔵しない人工肺を採用しており，体温調節機能の未発達な新生児では，導入開始後短時間で体温低下を併発する可能性がある。現在はプレコネクト化されていないこと，さらに遠心ポンプと回路はヘパリンコーティングされていないことなど，解決すべき問題は少なくはない。今回作成した新規システムは，熱交換器内蔵型人工肺の採用，プレコネクト化によるセットアップ時間の短縮，全血液接触面に対するヘパリンコーティング化を達成し，さらに現行システムより9mLの充填量削減が可能と考えられる。今回の24時間の急性動物実験において，システムの機能低下は観察されず良好なガス交換能を維持したことから，迅速導入用超低充填システムとしては十分な性能が示された。また，24時間の実験

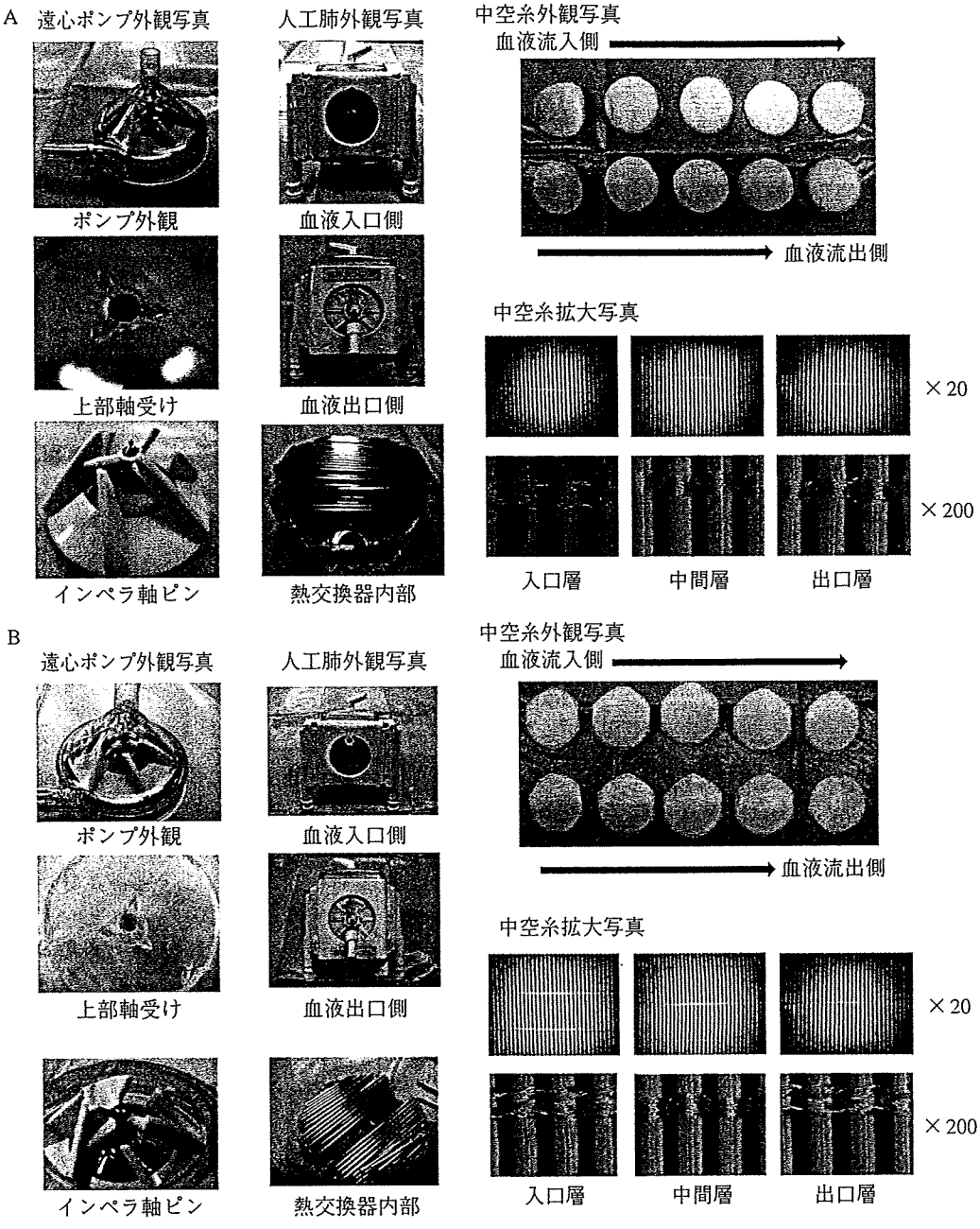


図8．実験終了後の遠心ポンプ・人工肺
A：Case 1
B：Case 2

を通じて人工肺からの血漿リークは観察されず，さらに長期に使用できる可能性も示唆された。血液成分の変化に関しては，ヘモグロビン濃度，血小板数は初期の血液希釈による影響を除けば生理的範囲で推移しており，赤血球損傷や血小板減少の少ないシステムであることが示された。ACTは，初期ヘパリンナトリウム投与の影響と考えられる実験開始後3時間までの延長を除いて目標とした150～200秒で維持し得たが，全血液接触面をヘパリンコーティングされた本システムにおいては，システム内部の血栓形成もこのACT調節下で十分に抑制することが可能であった。また，人工肺および遠心ポンプデバイスの機能低下も認めず，安定した状態で実験を完了することが可能であったことから，今後の臨床導入を考慮する条件が整ったものと考えられる。

## Ⅴ．結　語

現行の迅速導入用超低充填小児補助循環システムの問題点を改善した新規の迅速導入用超低充填小児補助循環システムを作成し，24時間の*in vivo*評価を行った。新規システムは新生児・乳児の循環器科領域，呼吸器科領域，救命救急領域における迅速導入用超低充填小児補助循環システムとして，十分な性能を有していることが示唆された。

## §　文　献


1）Conrad SA, Rycus PT, Dalton H : Extracorporeal life support registry report 2004. ASAIO J 2005;51: 4-10.

2）Yamasaki Y, Hayashi T, Nakatani T, et al : Early experience with low-prim extracorporeal membrane oxygenation support in children. ASIO J 2005;52: 110-4.

3）西田博，遠藤真弘，小柳仁：人工心肺回路の生体適合性向上を目指して－各種ヘパリンコーティングと新しいアプローチー．循環制御 1999;4(20):394-403.

4）大田圭，巽英介，片桐伸将，他：ヘパリンコーティング人工肺 Platinum Cube NCVC シリーズ開発の現状－Platinum Cube NCVC 2000の慢性動物実験による検討－．膜型肺2005;28:48-50.

5）Alsoufi B, Al-radi OO, Gruenwald BW, et al : Extracorporeal life support following cardiac surgery in children: analysis of risk factors and survival in a single institution. Eur J Cardiothorac Surg 2009;35: 1004-11.

6）Tajik M, Cardarelli MG : Extracorporeal membrane oxygenation after cardiac arrest in children : what do we know?. Eur J Cardiothorac Surg 2008;33:409-17.

7）上村秀樹，稲盛修二，林輝行，他：乳児におけるcatheter合併症に対処可能な超低充填量体外循環補助装置．日本小児循環器学会雑誌 2001; 17:646-7.

# 819　二葉式機械弁を用いた空気駆動式補助人工心臓内部における流れの可視化

## A Flow Visualization in a Pneumatic Ventricular Assist Device with a Bileaflet Mechanical Heart Valve

○学　金城 利晴 (阪府高専)　　李 桓成 (国循 研究所)　　巽 英介 (国循 研究所)
妙中 義之 (国循 研究所)　　正　上村 匡敬 (阪府高専)

Toshiharu KANESHIRO, Osaka Prefectural College of Technology, 26-12, Saiwai-cho, Neyagawa, Osaka
Hwansung LEE, National Cardiovascular Center
Eisuke TATSUMI, National Cardiovascular Center
Yoshiyuki TAENAKA, National Cardiovascular Center
Tadayuki KAMIMURA, Osaka Prefectural College of Technology

*Key Words*: Pneumatic Ventricular Assist Device, Bileaflet mechanical heart valve, Flow visualization

### 1. 緒言

近年，拍動型をはじめとする様々な補助人工心臓(以下VAD : Ventricular Assist Device)に関する研究が行われている．拍動型VADの研究において，血栓発生を防ぐために血液ポンプ内における洗い流し効果を得る目的で一葉式機械弁が使用されている．しかし臨床においては血流動特性に優れた二葉式機械弁の使用が進んでいることから，将来的に一葉式機械弁の安定供給が期待できないということが示唆されている[1]．

そこで本研究では，国立循環器病センター研究所において開発されている次世代空気駆動式VAD[2] に二葉式機械弁を装着し，流入側弁の取り付け角度の変化によるVAD内部の流れへの影響について検討を行い，二葉式機械弁における流入側弁の最適な取り付け角度を得ることを目的とした．特に，弁を通過しVAD内部に複雑な流れを形成させる流入側ポート付近における流れに関して検討した．

### 2. 流れの可視化実験

#### 2.1. 実験装置および回路

本実験では，流れの可視化を行うために実物の空気駆動式VADと同形状のアクリル製モデルポンプを製作し，機械弁は二葉式機械弁のSorin Bicarbon弁を使用した．ドノバン形模擬循環装置にモデルポンプを接続し，補助循環装置(東洋紡，VCT-30)で駆動させた．実験システムには，出力30[mJ/pulse]の波長532[nm]のNd:YAGレーザを持つPIVシステムを用いた．作動流体は，蒸留水と50vol%グリセリンの水溶液(粘性係数3.4[cP]，密度1120[kg/m$^3$]，温度37[℃])を使用し，トレーサ粒子として平均粒径50[μm]のポリスチレン粒子を使用した．

#### 2.2. 実験方法

モデルポンプおよび弁の取り付け角度についてFig. 1 に示す．本実験は，血液ポンプの流入側ポートの中心(Center)とそこから左右6[mm](Left, Right)の計3箇所にシート状のレーザ光を照射し，流出側弁は0[°]と一定にし，流入側弁の取り付け角度を0, 30, 45[°]と変化させ，血液ポンプの拍動周期における拡張期から収縮期について流れの可視化を行い(Fig. 1)，PIV解析ソフトを用いて流動解析を行った．

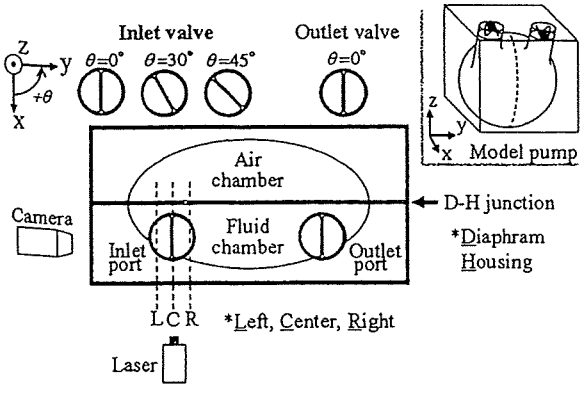


Fig. 1　Model pump and valve orientation angle

### 3. 実験結果および考察

血液ポンプの拡張期における流入側ポート付近の測定位置LeftでのPIV実験で得られた流速ベクトルの分布をFig. 2 に示す．Fig. 2 において破線で囲った箇所は，ダイアフラムとハウジングとの接合部(以下 D-H junction : Diaphram-Housing junction)付近への流速ベクトルを示している．

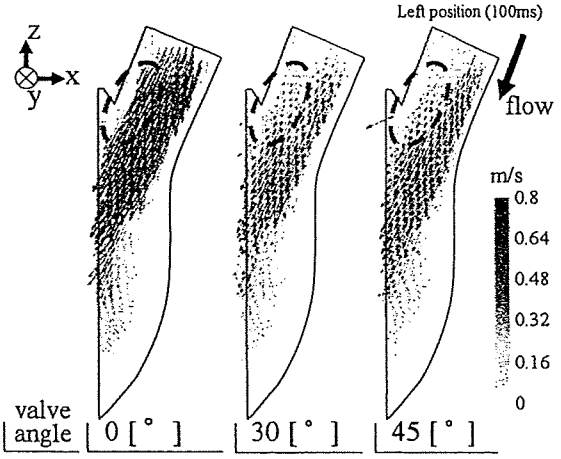


Fig. 2　Vector field of flow velocity at the inlet port

流入側弁の取り付け角度 0[°]において，D-H junction付近で流速が速いことがわかる．この流れによって，淀みの発生を防ぐ洗い流し効果が期待できると考えられる．

一方，流入側弁の取り付け角度 30, 45[°]においては，D-H junction付近での流れが遅いことがわかる．これにより，淀みが生じる恐れが予期される．原因としては，弁の取り付けに角度が付いてヒンジ軸がハウジングの曲壁面に接するようになることで，弁を通過した流体が壁面に沿うようにx方向へ流れてしまうためであると考えられる．

### 4. 結言

本研究では，流入側弁の取り付け角度の変化させることで血液ポンプ内部において異なる流動構造が観察された．流入側弁の取り付け角度0[°]では，D-H junction付近において流速が速いことから，淀みが生じることを防ぐ洗い流し効果が予測され血栓発生の抑制が期待される結果を得た．

以上より，本研究で用いた空気駆動式VADにおける流入側弁の取り付け角度は0[°]が最適であると考えられる．

### 参考文献

(1) Hwansung Lee, et al. , A Study on the Flow Visualization of a Mechanical Heart Valve in a Pneumatic Ventricular Assist Device, Proceeding of the 21th Bioengineering Conference of BED/JSME, pp.311-312,2009

(2) Akagawa Eiki, et al. , Effects of mechanical valve orifice direction on flow pattern in a ventricular assist device, J Artif Organs 10:85-91,2007

第日本機械学会講演論文集NO. 104 - 1('10.3 関西支部第 85 期定時総会講演会)

31st Annual International Conference of the IEEE EMBS
Minneapolis, Minnesota, USA, September 2-6, 2009

# Macroscopic Two-Pump Two-Vasculature Cardiovascular Model to Support Treatment of Acute Heart Failure

Masaru Sugimachi, *Member, IEEE*, Kenji Sunagawa, *Member, IEEE*,
Kazunori Uemura, Atsunori Kamiya, Shuji Shimizu, Masashi Inagaki and Toshiaki Shishido

*Abstract*— **Comprehensive understanding of hemodynamics remains a challenge even for expert cardiologists, partially due to a lack of an appropriate macroscopic model. We attempted to amend three major problems of Guyton's conceptual model (unknown left atrial pressure, unilateral heart damage, blood redistribution) and developed a comprehensive macroscopic model of hemodynamics that provides quantitative information. We incorporated a third axis of left atrial pressure, resulting in a 3D coordinate system. Pump functions of left and right heart are expressed by an integrated cardiac output curve, and the capacitive function of total vasculature by a venous return surface. The equations for both the cardiac output curve and venous return surface would facilitate precise diagnosis (especially evaluation of blood volume) and choice of appropriate treatments, including application to autopilot systems.**

## I. Introduction

COMPREHSNSIVE understanding of hemodynamics remains a challenge even for specialist clinicians including cardiologists. This is in part attributed to a lack of an appropriate macroscopic model of hemodynamics that would facilitate reasoning. Most cardiologists relied only on, if at all, the classical Guyton's circulatory equilibrium framework [1].

Guyton's model consists of only two subdivisions of the whole circulation: the cardiopulmonary component (in which both hearts and pulmonary vasculature are lumped) and the systemic vascular bed. These two subdivisions are characterized by the 'cardiac output curve' and 'venous return curve', respectively. The 'cardiac output curve' approximated the (total) pump function, and the 'venous return curve' approximated the capacitive function of systemic vasculature. The intersection of these curves coincides with the operating point of the circulation.

Guyton's model is, however, inappropriate (see MODEL AND METHODS) for the understanding of hemodynamics in patients with, for example, acute myocardial infarction, where only one ventricle is preferentially damaged. That is why many cardiologists gradually abandoned using Guyton's model for their reasoning.

If we can amend the shortcomings of Guyton's model and develop a more appropriate model, the new model would obviously help diagnosis procedures and treatment selection. Furthermore, the model may be able to quantify the hemodynamic abnormalities rather than just to identify them.

Therefore, the aim of this study was to develop a comprehensive macroscopic model of hemodynamics that would provide quantitative information and aid diagnosis and treatments.

Manuscript received April 7, 2009. This work was supported in part by Grant-in-Aid for Scientific Research (B 20300164, C 20500404) from the Ministry of Education, Culture, Sports, Science and Technology, by Health and Labour Sciences Research Grants (H19-nano-ippan-009, H20-katsudo -shitei-007) from the Ministry of Health Labour and Welfare of Japan.

M. Sugimachi, K. Uemura, A. Kamiya, S. Shimizu, M. Inagaki and T. Shishido are with the National Cardiovascular Center Research Institute, Suita, Osaka 5658565, Japan (corresponding author Masaru Sugimachi to provide phone: +81-6-6833-512; fax: +81-6-6835-5403; e-mail: su91mach@ri.ncvc.go.jp).

K. Sunagawa is with Kyushu University, Fukuoka 8128582 Japan. (e-mail: sunagawa@cardiol.med.kyushu-u.ac.jp).

## II. Model and Methods

### A. Shortcomings of Guyton's Model

Guyton's model has a number of problems when used in patients with unilateral heart failure.

First, the model does not provide left atrial pressure (LAP) values directly. LAP indicates the degree of pulmonary congestion and blood desaturation, and is as important as cardiac output (CO) and blood pressure.

Second, it is impossible to precisely model unilateral heart failure, which is frequently seen in patients with ischemic heart disease.

Third, in unilateral heart failure, the relative blood volumes in pulmonary and systemic vascular beds vary. As Guyton's model assumes only blood volume within the systemic vascular bed, such redistribution would shift the venous return curve even though the total blood volume remains the same.

### B. Development of Comprehensive Cardiovascular Model

To solve the above problems, we extended Guyton's model.

First, a third axis of LAP was introduced in our new model (Fig. 1) [2], [3], so that LAP can be obtained directly. The pumping ability of the heart and the capacitive function of the vasculature are expressed simultaneously in the 3D space (RAP-LAP-CO coordinate system).

Second, the pumping abilities of the left and right heart are expressed separately by the respective cardiac output surfaces that are independent of each other. In an equilibrium state, by matching the cardiac output of both sides, the pumping ability of the whole heart can be integrated and expressed by a curve

expressing the intersection of the two surfaces (integrated cardiac output curve, Fig. 1, thick curve).

Third, the capacitive function of total vasculature (including both systemic and pulmonary vasculatures) is expressed by the venous return surface (Fig. 1, shaded surface), which is an extension of the venous return curve. This surface expresses the changes in LAP and right atrial pressure (RAP) in response to CO change, while the total intravascular blood volume remains constant. In addition, blood redistribution between systemic and pulmonary vasculatures (without change in total blood volume) will be expressed by movement within the surface rather than by deviation from the surface.

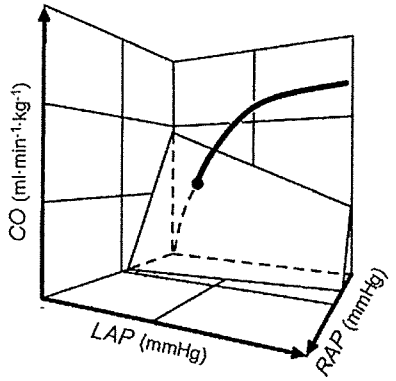


Fig. 1. An original macroscopic model of hemodynamics (an extended Guyton's model). The curve expresses the integrated pumping ability of left and right heart. The shaded surface characterizes the capacitive function of the total (systemic + pulmonary) vasculatures. The surface remains constant as long as the total intravascular blood volume remains the same. CO, cardiac output; LAP, left atrial pressure; RAP, right atrial pressure.

### *C. Animal Experiments to Characterize Venous Return Surface*

Figure 2 depicts the scheme of an experiment to characterize the venous return surface. We replaced the left and right heart with roller pumps, which allows us to change CO of the right heart or left heart independently.

By adjusting the flow (i.e., CO) of the two pumps to the same level, the changes in RAP and LAP in response to a change in CO can be observed. Blood redistribution between systemic and pulmonary vasculatures can be reproduced by transiently unbalancing the flow of the two pumps.

From each dog (n = 6), we obtained 6 different sets of data (CO, RAP, LAP). These data were subjected to bivariate linear regression using RAP and LAP as independent variables and CO as the dependent variable.

## III. RESULTS

Figure 3 illustrates the venous return surfaces obtained from 6 dogs. Bivariate linear regression in each animal yielded a flat surface in 3D space. The surface is shown as a line in Fig. 3, because we have projected the surface in a

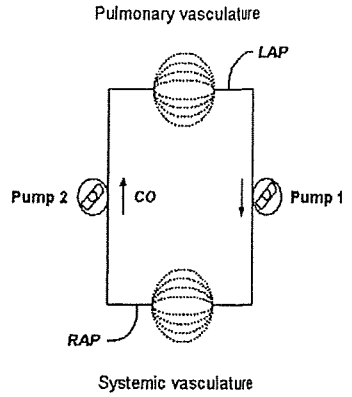


Fig. 2. An experimental scheme to characterize venous return surface. By replacing the left and right heart with roller pumps, one can change cardiac output of the right heart or left heart independently.

direction parallel to the surface. The experimental data obtained from each of the 6 animals showed good fit with the surface. In addition, the surfaces obtained from 6 animals were almost parallel, as shown by the nearly parallel 3D coordinate axes. These experimental results indicated that the venous return surface is linear and can be expressed by a common equation for all animals.

Further, by infusing or withdrawing known amounts of blood, we were able to derive an equation for the venous return surface as follows:

$$CO = V / 0.129 - 19.61\,RAP - 3.49\,LAP$$

where V is total intravascular stressed blood volume. This formula [$V = (CO + 19.61\,RAP + 3.49\,LAP) \times 0.129$] can be used to quantify V from CO, RAP and LAP.

We also succeeded to quantify the integrated cardiac output curve by logarithmic functions as follows:

$$CO = S_L\,[\ln(LAP-2.03)+0.80]$$

$$CO = S_R\,[\ln(RAP-2.13)+1.90]$$

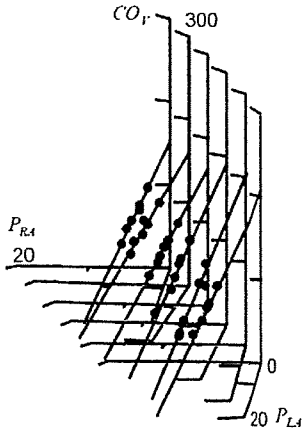


Fig. 3. Superimposed venous return surfaces obtained from 6 dogs. For each dog, the venous return surface (RAP-LAP-CO relationship) in 3D coordinate system was projected in a direction parallel to the surface, and was superimposed with each other.

where $S_L$ and $S_R$ are parameters expressing the pumping ability of the left and right heart, respectively. These equations are also useful for quantifying the pumping ability of right and left heart ($S_L$ = CO / [ln(LAP - 2.03) + 0.80], $S_R$ = CO / [ln(RAP - 2.13) + 1.90]).

Using this model, we are able to predict with acceptable precision the hemodynamics after infusion or withdrawal of known amounts of blood (CO: y = 0.93x + 6.5, $r^2$ = 0.96, SEE = 7.5 ml·min$^{-1}$·kg$^{-1}$; LAP: y = 0.90x + 0.5, $r^2$= 0.93, SEE = 1.4 mmHg; RAP: y = 0.87x + 0.4, $r^2$= 0.91, SEE = 0.4 mmHg) (Fig. 4) [3].

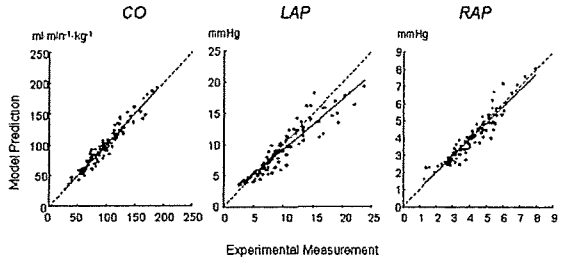


Fig. 4. Prediction of CO, LAP, and RAP based on our comprehensive macroscopic model of hemodynamics.

## IV. Discussion

### *A. Difficulty in Decision Making of Heart Failure Treatment*

Three hemodynamic variables: blood pressure, CO and LAP, appear to be the most essential factors influencing the survival of patients with heart failure. Our model clearly indicates that pump functions of left and right heart and total intravascular blood volume are determinants of CO and LAP. Systemic vascular resistance is an additional determinant of blood pressure.

For clinicians, the evaluation of blood volume is relatively difficult compared to pump functions and vascular resistance. In practice, clinicians have been using RAP as a proxy for blood volume. It is clear from our results [V = (CO + 19.61 RAP + 3.49 LAP) × 0.129] that blood volume (V) is not solely determined by RAP. Rather, all three parameters of CO, RAP and LAP are necessary to evaluate blood volume. The equation indicates that an increase of RAP by 1 mmHg is equivalent to an LAP increase of 5.6 mmHg, and a CO increase of 19.61 mL/min/kg (ca. 0.98 L/min for a 50-kg patient).

### *B. Application of the Model: Autopilot System*

The biggest benefit of our comprehensive visual model of hemodynamics is that it enables us to diagnose the abnormality of cardiovascular system in a quantitative manner. This would lead to appropriate selection of drugs and their doses.

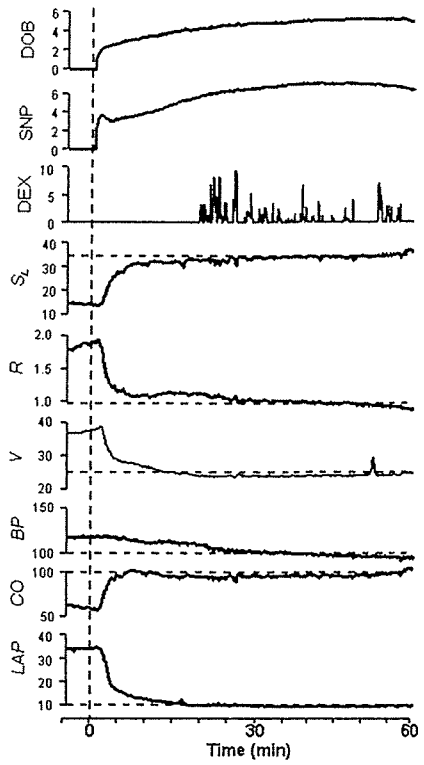


Fig. 5. An example of correction of hemodynamics with an autopilot system. By normalizing cardiovascular properties [pump function ($S_L$), resistance (R), blood volume (V)] with the administration of dobutamine (DOB), sodium nitroprusside (SNP), and dextran 40 solution (DEX), all the abnormal hemodynamic variables (increased blood pressure [BP], decreased cardiac output [CO], and elevated left atrial pressure [LAP]) were resolved rapidly, sufficiently, and stably.

As shown in Fig. 5, by translating hemodynamic variables into cardiovascular properties (pump function, vascular resistance, and blood volume), and by controlling each of these parameters with individual drug with preferential effect on the parameter, we are able to correct automatically all the parameters of blood pressure, CO and LAP rapidly, stably, and simultaneously.

Using an autopilot system to administer dobutamine (DOB at 5 ± 3 mg·kg$^{-1}$·min$^{-1}$), nitroprusside (SNP at 4 ± 2 mg·kg$^{-1}$·min$^{-1}$), dextran infusion (DEX at 2 ± 2 ml·kg$^{-1}$), and furosemide (10 mg in one, 20 mg in one) in 12 dogs with acute heart failure rapidly normalized blood pressure, CO, and LAP in 5 ± 7, 7 ± 5, and 12 ± 10 minutes, respectively. The normalized values remained stable thereafter (RMS values, blood pressure = 4 ± 3 mmHg, CO = 5 ± 2 ml·min$^{-1}$·kg$^{-1}$, LAP = 0.8 ± 0.6 mmHg).

## V. Conclusion

We have successfully developed a comprehensive macroscopic model of hemodynamics that provides quantitative information. Using a 3D coordinate system, the pump functions of left and right heart are expressed by an

integrated cardiac output curve, and the capacitive function of total vasculature by a venous return surface. The equations of both the cardiac output curve and venous return surface would facilitate accurate diagnosis (especially evaluation of blood volume) and choice of appropriate treatments, including application to autopilot systems.

## REFERENCES


[1] A. C. Guyton, "Determination of cardiac output by equating venous return curves with cardiac response curves," *Physiol. Rev.* vol. 35, no. 1,123–129, Jan. 1955.

[2] K. Uemura, M. Sugimachi, T. Kawada, A. Kamiya, Y. Jin, *et al.*, "A novel framework of circulatory equilibrium," *Am. J. Physiol. Heart Circ. Physiol.* vol. 286, no. 6, pp. H2376–H2385, Jun. 2004.

[3] K. Uemura, T. Kawada, A. Kamiya, T. Aiba, I. Hidaka, *et al.*, "Prediction of circulatory equilibrium in response to changes in stressed blood volume," *Am. J. Physiol. Heart Circ. Physiol.* vol. 289, no. 1, H301–H307, Jul. 2005.

*Am J Physiol Heart Circ Physiol* 296: H1666–H1674, 2009.
First published February 27, 2009; doi:10.1152/ajpheart.01041.2008.

# Angiotensin II disproportionally attenuates dynamic vagal and sympathetic heart rate controls

**Toru Kawada,[1] Masaki Mizuno,[1] Shuji Shimizu,[2] Kazunori Uemura,[1] Atsunori Kamiya,[1] and Masaru Sugimachi[1]**

[1]*Department of Cardiovascular Dynamics, Advanced Medical Engineering Center, National Cardiovascular Center Research Institute, Osaka and* [2]*Japan Association for the Advancement of Medical Equipment, Tokyo, Japan*

Submitted 29 September 2008; accepted in final form 25 February 2009

**Kawada T, Mizuno M, Shimizu S, Uemura K, Kamiya A, Sugimachi M.** Angiotensin II disproportionally attenuates dynamic vagal and sympathetic heart rate controls. *Am J Physiol Heart Circ Physiol* 296: H1666–H1674, 2009. First published February 27, 2009; doi:10.1152/ajpheart.01041.2008.—To better understand the pathophysiological role of angiotensin II (ANG II) in the dynamic autonomic regulation of heart rate (HR), we examined the effects of intravenous administration of ANG II (10 $\mu g \cdot kg^{-1} \cdot h^{-1}$) on the transfer function from vagal or sympathetic nerve stimulation to HR in anesthetized rabbits with sinoaortic denervation and vagotomy. In the vagal stimulation group ($n$ = 7), we stimulated the right vagal nerve for 10 min using binary white noise (0–10 Hz). The transfer function from vagal stimulation to HR approximated a first-order low-pass filter with pure delay. ANG II attenuated the dynamic gain from 7.6 ± 0.9 to 5.8 ± 0.9 beats·$min^{-1}$·$Hz^{-1}$ (means ± SD; $P <$ 0.01) without affecting the corner frequency or pure delay. In the sympathetic stimulation group ($n$ = 7), we stimulated the right postganglionic cardiac sympathetic nerve for 20 min using binary white noise (0–5 Hz). The transfer function from sympathetic stimulation to HR approximated a second-order low-pass filter with pure delay. ANG II slightly attenuated the dynamic gain from 10.8 ± 2.6 to 10.2 ± 3.1 beats·$min^{-1}$·$Hz^{-1}$ ($P$ = 0.049) without affecting the natural frequency, damping ratio, or pure delay. The disproportional suppression of the dynamic vagal and sympathetic regulation of HR would result in a relative sympathetic predominance in the presence of ANG II. The reduced high-frequency component of HR variability in patients with cardiovascular diseases, such as myocardial infarction and heart failure, may be explained in part by the peripheral effects of ANG II on the dynamic autonomic regulation of HR.

systems analysis; transfer function; heart rate variability; cardiac sympathetic nerve activity; rabbit

AUTONOMIC NERVOUS ACTIVITY changes dynamically during daily activity, and thus the dynamic heart rate (HR) regulation by the autonomic nervous system is physiologically important. The high-frequency (HF) component of HR variability (HRV) is thought to reflect primarily vagal nerve activity, because the vagal nerve can change the HR more quickly than the sympathetic nerve (1, 3, 14, 34). This does not mean, however, that the sympathetic system cannot affect the HF component. For example, an increase in background sympathetic tone augments the HR response to vagal stimulation, an effect that has been referred to as accentuated antagonism (20). In accordance with accentuated antagonism, selective cardiac sympathetic nerve stimulation augments the dynamic HR response to vagal stimulation (14). On the other hand, high plasma concentration of norepinephrine (NE) with no direct activation of the cardiac sympathetic nerve attenuates the dynamic HR response to vagal stimulation via an α-adrenergic mechanism (24). These results suggest that the sympathetic system can influence the HF component via complex interactions with the vagal system.

During systemic sympathetic activation, the renin-angiotensin system is activated through stimulation of $\beta_1$-adrenergic receptors on juxtaglomerular granular cells (8, 12). In such conditions as hypertension, myocardial ischemia, and heart failure, the renin-angiotensin system and the sympathetic nervous system are both activated (9, 35). Previous studies demonstrated that acute intravenous or intracerebroventricular administration (32) or chronic intravenous administration of angiotensin II (ANG II) modified the baroreflex control of HR in rabbits (5), possibly via a decrease in vagal tone and an increase in sympathetic tone to the heart. In the present study, we focused on the peripheral effects of ANG II and examined the effects of intravenous ANG II on the dynamic HR response to vagal or postganglionic cardiac sympathetic nerve stimulation. In a previous study from our laboratory where anesthetized cats were used, intravenous ANG II (10 $\mu g \cdot kg^{-1} \cdot h^{-1}$) attenuated myocardial interstitial acetylcholine (ACh) release in response to vagal nerve stimulation (17); therefore, we hypothesized that intravenous ANG II at this dose would attenuate the dynamic HR response to vagal nerve stimulation. On the other hand, a previous study from our laboratory where anesthetized rabbits were used demonstrated that intravenous ANG II at a similar dose of 6 $\mu g \cdot kg^{-1} \cdot h^{-1}$ did not affect the peripheral arc transfer function estimated between renal sympathetic nerve activity and arterial pressure (AP) (13). Accordingly, we hypothesized that intravenous administration of ANG II would not modulate the dynamic sympathetic control of HR significantly. We focused on the relative effects of ANG II on the vagal and sympathetic HR regulations because the balance between vagal and sympathetic nerve activities would be a key to understanding the pathophysiology of several cardiovascular diseases.

## MATERIALS AND METHODS

*Surgical preparations.* Animal care was performed in accordance with *Guideline Principles for the Care and Use of Animals in the Field of Physiological Sciences*, which has been approved by the Physiological Society of Japan. All experimental protocols were reviewed and approved by the Animal Subjects Committee at the National Cardiovascular Center. Twenty-one Japanese white rabbits weighing 2.4–3.4 kg were anesthetized with intravenous injections (2 ml/kg) of a mixture of urethane (250 mg/ml) and α-chloralose (40 mg/ml) and mechanically ventilated with oxygen-enriched room air. A double-lumen catheter was inserted into the right femoral vein, and a supplemental dose of the anesthetics was given continuously (0.5–1.0

Address for reprint requests and other correspondence: T. Kawada, Dept. of Cardiovascular Dynamics, Advanced Medical Engineering Center, National Cardiovascular Center Research Institute, 5-7-1 Fujishirodai, Suita, Osaka 565-8565, Japan (e-mail: torukawa@res.ncvc.go.jp).

$ml \cdot kg^{-1} \cdot h^{-1}$). AP was monitored using a micromanometer catheter (Millar Instruments, Houston, TX) inserted into the right femoral artery. HR was determined from the electrocardiogram using a cardiotachometer. Sinoaortic denervation and vagotomy were performed bilaterally to minimize reflex changes in efferent sympathetic nerve activity. The left and right cardiac sympathetic nerves were exposed using a midline thoracotomy and sectioned (16). In the vagal stimulation group, a pair of bipolar stainless steel wire electrodes was attached to the cardiac end of the sectioned right vagal nerve for stimulation. A pair of stainless steel wire electrodes was attached to the proximal end of the sectioned right cardiac sympathetic nerve for recording efferent cardiac sympathetic nerve activity (CSNA). In the sympathetic stimulation group, a pair of bipolar stainless steel wire electrodes was attached to the cardiac end of the sectioned right sympathetic nerve for stimulation. Efferent CSNA was recorded from the proximal end of the sectioned left cardiac sympathetic nerve. The preamplified nerve signal was band-pass filtered between 150 and 1,000 Hz. The signal was then full-wave rectified and low-pass filtered with a cut-off frequency of 30 Hz to quantify the nerve activity. Both the stimulation and recording electrodes were fixed to the nerve by addition-curing silicone glue (Kwik-Sil; World Precision Instruments, Sarasota, FL). We confirmed that the recorded CSNA was mainly postganglionic by observing the disappearance of CSNA following intravenous administration of hexamethonium bromide (50 mg/kg) at the end of each experiment. The body temperature of the animal was maintained at 38°C with a heating pad throughout the experiment.

*Protocols.* In the vagal stimulation group ($n = 7$), the stimulation amplitude was adjusted (3–6 V) in each animal to yield a HR decrease of ~50 beats/min at 5-Hz tonic stimulation with a pulse duration of 2 ms. To estimate the transfer function from vagal stimulation to HR, a random vagal stimulus was applied for 10 min by altering the stimulus command every 500 ms at either 0 or 10 Hz according to a binary white noise signal. The input power spectral density was relatively constant up to 1 Hz, which covered the upper frequency range of interest with respect to the vagal transfer function in rabbits (26).

In the sympathetic stimulation group ($n = 7$), the stimulation amplitude was adjusted (1–3 V) in each animal to yield a HR increase of ~50 beats/min at 5-Hz tonic stimulation with a pulse duration of 2 ms. To estimate the transfer function from sympathetic stimulation to HR, a random sympathetic stimulus was applied for 20 min by altering the stimulus command every 2 s at either 0 or 5 Hz according to a binary white noise signal. The input power spectral density was relatively constant up to 0.25 Hz, which covered the upper frequency range of interest with respect to the sympathetic transfer function in rabbits (15).

In both the vagal stimulation and sympathetic stimulation groups, the dynamic HR response to nerve stimulation was first recorded under conditions of continuous intravenous infusion of physiological saline solution ($1\ ml \cdot kg^{-1} \cdot h^{-1}$). After the control data were recorded, nerve stimulation was stopped and ANG II was intravenously administered at $10\ \mu g \cdot kg^{-1} \cdot h^{-1}$ ($1\ ml \cdot kg^{-1} \cdot h^{-1}$ of 10 μg/ml solution) instead of the physiological saline solution. After 15 min, we repeated the random stimulation of the vagal or sympathetic nerve while continuing the intravenous injection of ANG II. We used the same binary white noise sequence for the control and ANG II conditions in each animal and changed the sequence for different animals.

In a supplemental protocol ($n = 7$), we examined the time effect on the estimation of the sympathetic transfer function. The 20-min random sympathetic stimulation was repeated twice with an intervening interval of more than 20 min.

*Data analysis.* Data were digitized at 200 Hz using a 16-bit analog-to-digital converter and stored on the hard disk of a dedicated laboratory computer system. Prestimulation values of HR, AP, and CSNA were calculated by averaging data obtained during the 10 s immediately before nerve stimulation. The mean HR and AP values in response to nerve stimulation were calculated by averaging data obtained during the nerve stimulation period. The mean level of CSNA during the nerve stimulation period was not evaluated because contamination from stimulation artifacts could not be completely eliminated.

The transfer function from nerve stimulation to the HR response was estimated as follows. The input-output data pairs of nerve stimulation and HR were resampled at 10 Hz. To avoid the initial transition from no stimulation to random stimulation biased the transfer function estimation, data were processed only from 2 min after the initiation of random stimulation. In the vagal stimulation group, the data were divided into eight segments of 1,024 data points that half-overlapped with neighboring segments. In the sympathetic stimulation group, the data were divided into eight segments of 2,048 data points that half-overlapped with neighboring segments. For each segment, a linear trend was subtracted and a Hanning window was applied. We then performed a fast Fourier transformation to obtain the frequency spectra of the stimulation command [$X(f)$] and HR [$HR(f)$] (4). We calculated ensemble averages of the power spectral densities of the stimulation command [$S_{X \cdot X}(f)$] and HR [$S_{HR \cdot HR}(f)$] and the cross spectral density between the two signals [$S_{HR \cdot X}(f)$]. Finally, we obtained the transfer function [$H(f)$] from the nerve stimulation to HR response using the following equation (23):

$$H(f) = \frac{S_{HR \cdot X}(f)}{S_{X \cdot X}(f)}$$

To quantify the linear dependence of the HR response to vagal or sympathetic nerve stimulation, we estimated the magnitude-squared coherence function [$Coh(f)$] using the following equation (23):

$$Coh(f) = \frac{|S_{HR \cdot X}(f)|^2}{S_{X \cdot X}(f) \cdot S_{HR \cdot HR}(f)}$$

The coherence function ranges zero and unity and indicates a frequency-domain measure of linear dependence between input and output variables.

Because previous studies found that the transfer function from vagal stimulation to HR approximated a first-order low-pass filter with pure delay (14, 24), we determined the parameters of the vagal transfer function using the following model:

$$H_{vagus}(f) = -\frac{K}{1 + \frac{f}{f_C} j} e^{-2\pi f j L}$$

where $K$ is dynamic gain (in $beats \cdot min^{-1} \cdot Hz^{-1}$), $f_C$ is the corner frequency (in Hz), and $L$ is pure delay (in s). Variables $f$ and $j$ represent frequency and an imaginary unit, respectively. The minus sign in the right side of the equation corresponds to the negative HR response to vagal stimulation.

Because previous studies suggested that the transfer function from sympathetic stimulation to HR approximated a second-order low-pass filter with pure delay (14, 28), we determined the parameters of the sympathetic transfer function using the following model:

$$H_{symp}(f) = \frac{K}{1 + 2\zeta \frac{f}{f_N} j + \left(\frac{f}{f_N} j\right)^2} e^{-2\pi f j L}$$

where $K$ is dynamic gain (in $beats \cdot min^{-1} \cdot Hz^{-1}$), $f_N$ is the natural frequency (in Hz), $\zeta$ is the damping ratio, and $L$ is pure delay (in s).

Because deviation of the model transfer function [$H_{model}(f)$] from the estimated transfer function [$H_{est}(f)$] would affect the transfer function parameters, we assessed the goodness of fit using the following equation:

$$\text{Goodness of Fit (\%)} = 100 \times \left[1 - \left(\sum_{m=1}^{N} \frac{|H_{model}(f) - H_{est}(f)|^2}{m}\right) \Big/ \left(\sum_{m=1}^{N} \frac{|H_{est}(f)|^2}{m}\right)\right]$$

$$f = f_0 \times m$$

where $f_0$, $m$, and $N$ represent the fundamental frequency of the Fourier transformation, a frequency index, and the number of data points used for the fitting, respectively. When $H_{model}(f)$ is zero for all of the frequencies, the goodness of fit is zero. When $H_{model}(f)$ equals $H_{est}(f)$ for all of the frequencies, the goodness of fit is 100%.

To facilitate intuitive understanding of the dynamic characteristics described by the transfer function (see Appendix A for details), we calculated the step response from the corresponding transfer function as follows. An impulse response of the system was calculated using the inverse Fourier transformation of the estimated transfer function. The step response was then obtained from the time integral of the impulse response. The steady-state response was calculated by averaging the last 10 s of data from the step response. The 80% rise time for the sympathetic step response or the 80% fall time for the vagal step response was estimated as the time at which the step response reached 80% of the steady-state response.

*Statistics.* All data are presented as means and SD values. Mean values of HR, AP, and CSNA as well as parameters of the transfer functions and step responses were compared between the control and ANG II conditions using paired *t*-tests. Differences were considered significant when $P < 0.05$ (11).

## RESULTS

Typical recordings of the vagal stimulation command, HR, and AP obtained under control and ANG II conditions are shown in Fig. 1*A*. The random vagal stimulation began at 60 s. The HR decreased in response to the random vagal stimulation. ANG II, which did not affect the prestimulation baseline HR, attenuated the magnitude of the vagal stimulation-induced variations in HR. ANG II increased the AP both before and during the vagal stimulation. ANG II did not change the prestimulation or poststimulation CSNA (Fig. 1*B*).

As shown in Table 1, ANG II did not affect the mean HR before stimulation of the vagal nerve, whereas it significantly increased the mean HR during the vagal stimulation period. ANG II attenuated the reduction in HR, which was calculated as the difference between the prestimulation HR and the mean HR observed during the vagal stimulation period. ANG II significantly increased the mean AP both before and during the vagal stimulation period. ANG II did not affect the mean level of pre- or poststimulation CSNA significantly.

Figure 2*A* illustrates the averaged transfer functions from vagal stimulation to HR obtained under the control and ANG II conditions. In the gain plots, the transfer gain was relatively constant for frequencies below 0.1 Hz and decreased as the frequency increased above 0.1 Hz. ANG II decreased the transfer gain for all of the investigated frequencies, resulting in

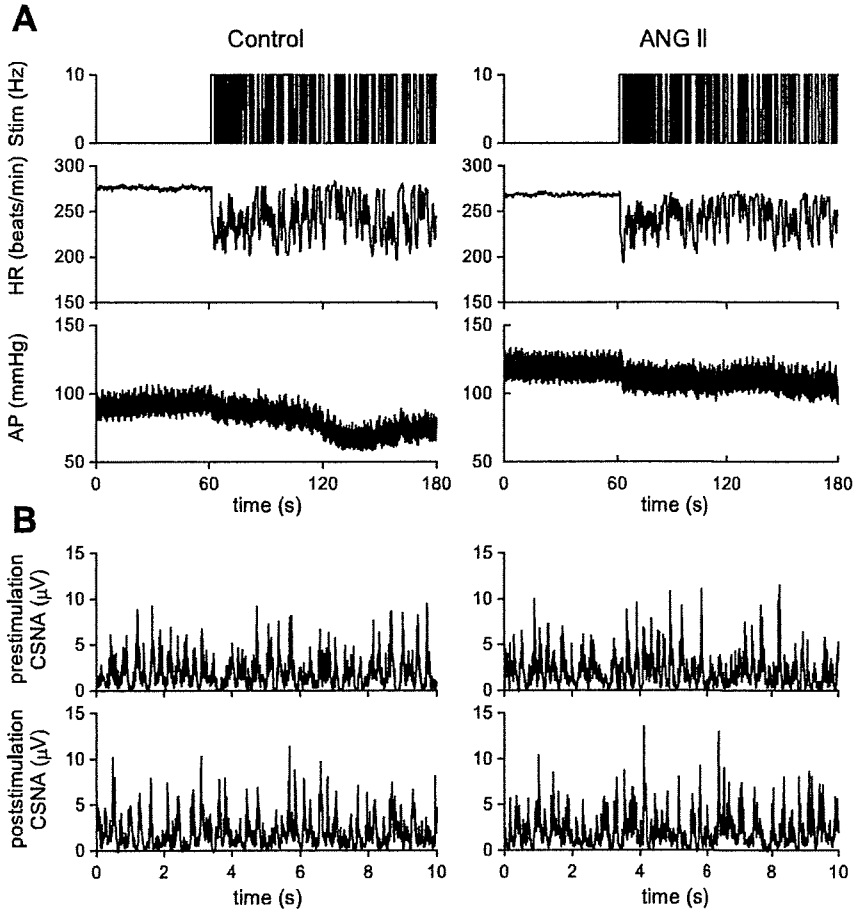


Fig. 1. *A*: representative recordings of vagal nerve stimulation (Stim), the heart rate (HR), and arterial pressure (AP). The *left* and *right* panels show recordings obtained before and during intravenous administration of angiotensin II (ANG II; 10 $\mu g \cdot kg^{-1} \cdot h^{-1}$), respectively. The amplitude of the HR variation in response to vagal stimulation was smaller in the presence of ANG II compared with results obtained without ANG II. *B*: representative recordings of cardiac sympathetic nerve activity (CSNA) under prestimulation baseline and poststimulation conditions. ANG II did not affect the CSNA significantly.

Table 1. *Mean values for HR, AP, and CSNA obtained using the vagal stimulation protocol*

| | Control | ANG II | *P* Value |
|---|---|---|---|
| HR, beats/min | | | |
| Prestimulation | 278±21 | 281±31 | 0.60 |
| During stimulation | 232±19 | 245±26* | 0.046 |
| Difference‡ | −46±6 | −37±10† | 0.0017 |
| AP, mmHg | | | |
| Prestimulation | 91±23 | 127±17† | 0.0057 |
| During stimulation | 85±24 | 118±19† | 0.0055 |
| Difference‡ | −6.3±9.2 | −9.2±8.6 | 0.34 |
| CSNA, μV | | | |
| Prestimulation | 1.21±0.38 (100%) | 1.19±0.46 (98±15%) | 0.82 |
| Poststimulation | 1.27±0.42 (105±8%) | 1.20±0.55 (98±27%) | 0.59 |

Data are means ± SD values; $n = 7$. HR, heart rate; AP, arterial pressure; CSNA, cardiac sympathetic nerve activity. ‡The difference was calculated by subtracting the prestimulation value from the value obtained during the vagal stimulation period in each animal. *$P < 0.05$ and †$P < 0.01$ based on a paired *t*-test. Exact *P* values are also shown.

a parallel downward shift in the gain plot. In the phase plots, the phase approached $-\pi$ radians at 0.01 Hz and the lag became larger as the frequency increased. ANG II did not alter the phase characteristics significantly. In the coherence plots, the coherence value was close to unity in the frequency range from 0.01 to 0.8 Hz. The sharp variation around 0.6 Hz corresponds to the frequency of the artificial ventilation. Figure 2*B* depicts the HR step responses calculated from the corresponding transfer functions. ANG II significantly attenuated the steady-state response without affecting the response speed.

As shown in Table 2, ANG II significantly attenuated the dynamic gain of the vagal transfer function to 76.1 ± 8.5% of the control value without affecting the corner frequency or pure delay. The goodness of fit to the first-order low-pass filter did not differ between the control and ANG II conditions. In the HR step response, ANG II significantly attenuated the steady-state response without affecting the 80% fall time.

Typical recordings of the sympathetic stimulation command, HR, and AP obtained under control and ANG II conditions are shown in Fig. 3*A*. The random sympathetic stimulation began at 60 s. HR increased in response to random sympathetic stimulation. ANG II did not affect the prestimulation baseline HR. The magnitude of the HR variation in response to sympathetic stimulation did not change significantly. ANG II increased the AP both before and during the sympathetic stimulation. ANG II did not change the pre- or poststimulation CSNA significantly (Fig. 3*B*).

As shown in Table 3, ANG II did not affect the mean HR before or during the period of sympathetic stimulation. ANG II did not affect the increase in HR, calculated as the difference between the prestimulation HR and the mean HR in response to sympathetic stimulation. ANG II significantly increased the mean AP both before and during the sympathetic stimulation period. ANG II did not affect the mean level of pre- or poststimulation CSNA significantly.

Figure 4*A* illustrates the averaged transfer functions from sympathetic stimulation to HR obtained under control and ANG II conditions. In the gain plots, the transfer gain decreased as the frequency increased. ANG II did not change the transfer gain markedly. In the phase plots, the phase approached zero radians at 0.01 Hz and increasingly lagged as the frequency increased. ANG II did not affect the phase characteristics significantly. The coherence value was above 0.9 for the frequency range below 0.1 Hz and decreased in the frequency range above 0.1 Hz. Figure 4*B* depicts the HR step responses calculated from the corresponding transfer functions. ANG II did not affect the steady-state response or the response speed.

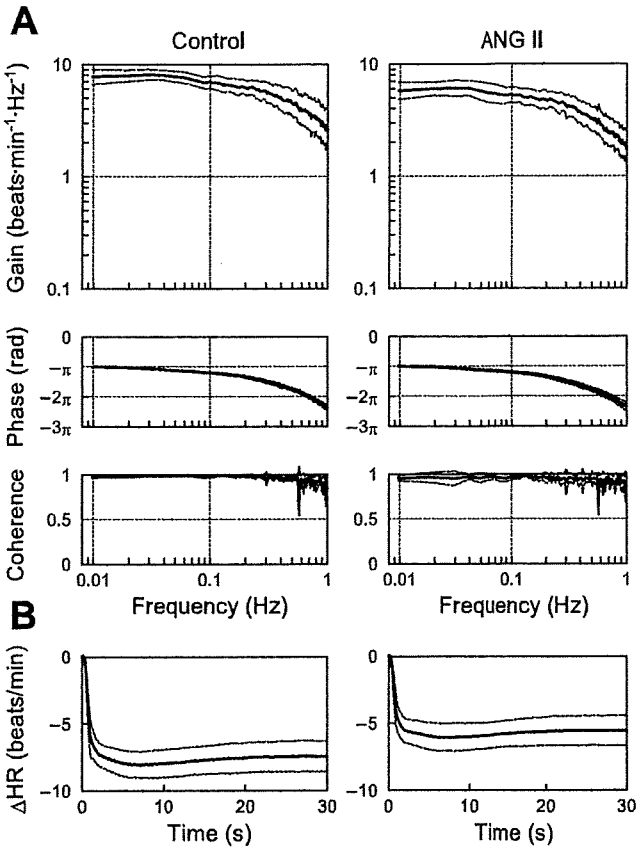


Fig. 2. *A*: averaged transfer functions from vagal nerve stimulation to the HR response obtained before and during intravenous administration of ANG II. Gain plots (*top*), phase plots (*middle*), and coherence plots (*bottom*) are shown. ANG II caused a parallel downward shift in the gain plot. ANG II did not affect the phase plot or coherence plot significantly. *B*: step responses of the HR to a unit change in the vagal stimulation calculated from the corresponding transfer functions. ANG II significantly attenuated the step response of the HR. ΔHR, changes in heart rate. Solid lines indicate mean, and dashed lines indicate mean ± SD.

Table 2. *Effects of ANG II on the parameters of the transfer function and the step response relating to the dynamic vagal control of HR*

| | Control | ANG II | *P* Value |
|---|---|---|---|
| Dynamic gain, beats·min$^{-1}$·Hz$^{-1}$ | 7.6±0.9 | 5.8±0.9* | 0.00042 |
| Corner frequency, Hz | 0.39±0.12 | 0.36±0.10 | 0.12 |
| Pure delay, s | 0.48±0.04 | 0.47±0.06 | 0.82 |
| Goodness of fit, % | 98.8±0.4 | 98.6±0.8 | 0.63 |
| Steady-state response, beats/min | −7.4±1.1 | −5.6±1.1* | 0.0011 |
| 80% Fall time | 1.31±0.31 | 1.33±0.37 | 0.60 |

Data are means ± SD values; $n = 7$. *$P < 0.01$ based on a paired *t*-test. Exact *P* values are also shown.

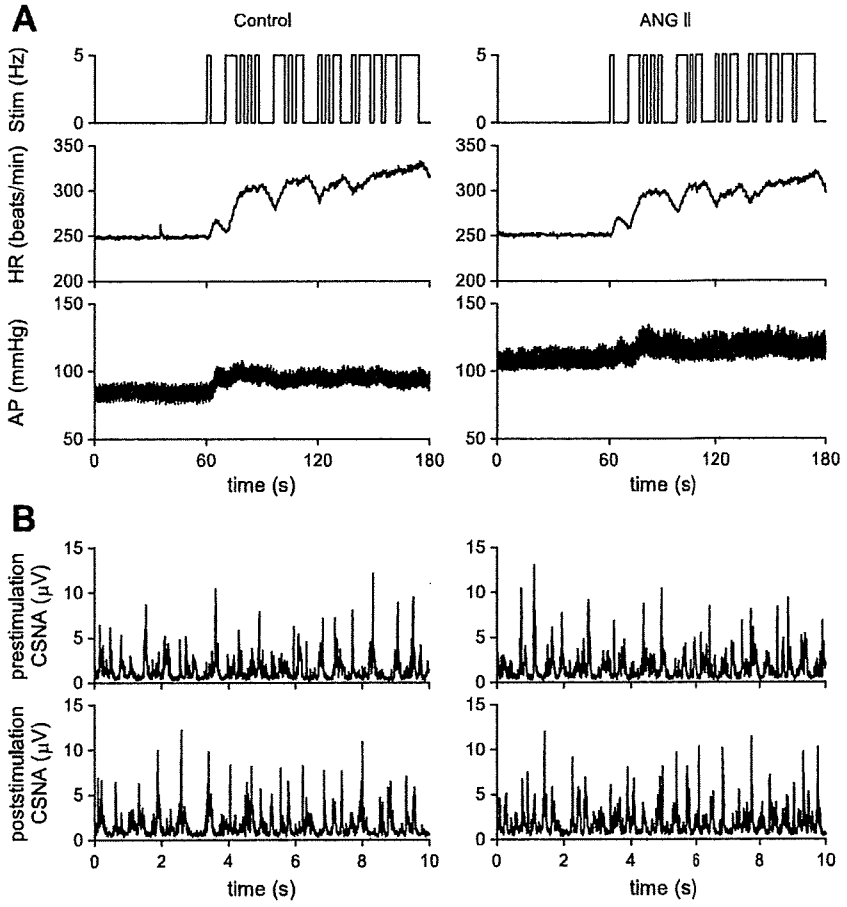


Fig. 3. *A*: representative recordings of cardiac sympathetic nerve stimulation (Stim), HR, and AP. The *left* and *right* panels show the recordings before and during intravenous administration of ANG II (10 $\mu g \cdot kg^{-1} \cdot h^{-1}$), respectively. The amplitude of the HR variation during sympathetic stimulation was unchanged by the addition of ANG II. *B*: representative recordings of CSNA under prestimulation baseline and poststimulation conditions. ANG II did not affect the CSNA significantly.

As shown in Table 4, ANG II slightly attenuated the dynamic gain of the sympathetic transfer function to 92.5 ± 8.9% of the value observed under control conditions. ANG II did not affect the natural frequency, damping ratio, or pure delay. The goodness of fit to the second-order low-pass filter did not differ between the control and ANG II conditions. In the HR step response, ANG II did not affect the steady-state response or the 80% rise time. As shown in Table 5, there were no significant differences in the parameters of the sympathetic transfer function between repeated estimations with an intervening interval of more than 20 min.

Table 3. *Mean values for HR, AP, and CSNA obtained using the sympathetic stimulation protocol*

| | Control | ANG II | *P* Value |
|---|---|---|---|
| HR, beats/min | | | |
| Prestimulation | 267±16 | 261±19 | 0.21 |
| During stimulation | 317±26 | 311±23 | 0.063 |
| Difference† | 50±21 | 50±21 | 0.94 |
| AP, mmHg | | | |
| Prestimulation | 74±6 | 106±15* | 0.0011 |
| During stimulation | 78±6 | 110±17* | 0.0023 |
| Difference† | 4.7±3.6 | 4.1±5.4 | 0.71 |
| CSNA, μV | | | |
| Prestimulation | 0.91±0.71 (100%) | 0.98±0.78 (99±19%) | 0.22 |
| Poststimulation | 0.93±0.72 (101±4%) | 1.02±0.81 (104±21%) | 0.18 |

Data are means ± SD values; $n = 7$ except for CSNA data where $n = 5$. †The difference was calculated by subtracting the prestimulation value from the value obtained during the sympathetic stimulation period in each animal. *$P < 0.01$ based on a paired *t*-test. Exact *P* values are also shown.

## DISCUSSION

Intravenous administration of ANG II at 10 $\mu g \cdot kg^{-1} \cdot h^{-1}$ increased AP but did not affect mean HR or mean CSNA during prestimulation baseline conditions (Tables 1 and 3), suggesting that ANG II at this dose did not affect the residual sympathetic tone to the heart significantly. ANG II significantly attenuated the dynamic gain of the transfer function from vagal stimulation to HR, whereas it only slightly attenuated that of the transfer function from sympathetic stimulation to HR (Tables 2 and 4).

*Effects of ANG II on the transfer function from vagal stimulation to HR.* ANG II attenuated the dynamic gain of the transfer function from vagal stimulation to HR without affecting the corner frequency or pure delay (Fig. 2 and Table 2). Several interventions can affect the dynamic gain of the vagal transfer function and significantly change the corner frequency. For example, inhibition of cholinesterase, which interferes with the rapid hydrolysis of ACh, augments the dynamic gain and decreases the corner frequency (29). Moreover, blockade of muscarinic $K^+$ channels, which interferes with fast, membrane-delimited signal transduction, has been shown to attenuate the dynamic gain and decrease the corner frequency (26).

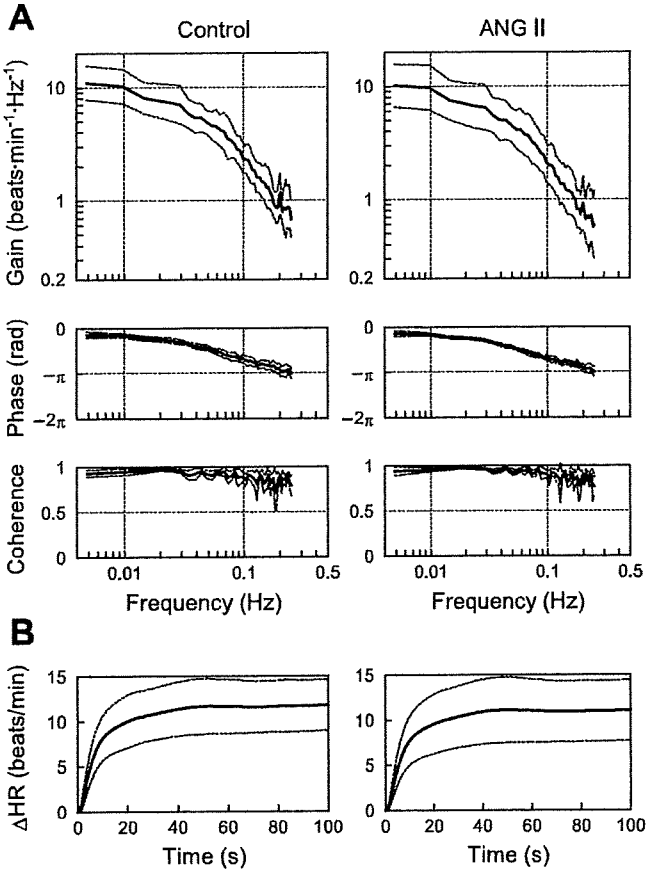


Fig. 4. *A*: averaged transfer functions from cardiac sympathetic nerve stimulation to the HR response obtained before and during intravenous administration of ANG II. Gain plots (*top*), phase plots (*middle*), and coherence plots (*bottom*) are shown. *B*: step responses of the HR to a unit change in the sympathetic stimulation calculated using the transfer functions. ΔHR, changes in heart rate. Solid lines indicate mean, and dashed lines indicate mean ± SD.

On the other hand, several other interventions have been shown to alter the dynamic gain of the vagal transfer function without changing the corner frequency. Concomitant cardiac sympathetic nerve stimulation or increased intracellular cyclic AMP levels augments the dynamic gain without affecting the corner frequency (14, 27), whereas β-adrenergic blockade or high plasma NE attenuates the dynamic gain without affecting the corner frequency (24, 25). Because α-adrenergic blockade nullifies its effects, high plasma NE probably functions via

Table 4. *Effects of intravenous ANG II administration on the parameters of the transfer function and the step response relating to the dynamic sympathetic control of HR*

| | Control | ANG II | *P* Value |
|---|---|---|---|
| Dynamic gain, beats·min$^{-1}$·Hz$^{-1}$ | 10.8±2.6 | 10.2±3.1* | 0.049 |
| Natural frequency, Hz | 0.069±0.009 | 0.065±0.006 | 0.090 |
| Damping ratio | 1.53±0.25 | 1.48±0.21 | 0.26 |
| Pure delay, s | 0.51±0.31 | 0.42±0.18 | 0.20 |
| Goodness of fit, % | 97.0±1.6 | 96.9±1.7 | 0.67 |
| Steady-state response, beats/min | 11.8±2.8 | 11.1±3.4 | 0.052 |
| 80% Rise time, s | 17.2±4.7 | 16.8±4.5 | 0.62 |

Data are means ± SD; $n = 7$. *$P < 0.05$ based on a paired *t*-test. Exact *P* values are also shown.

Table 5. *Time effects on the parameters of the transfer function and the step response relating to the dynamic sympathetic control of HR*

| | Control 1 | Control 2 | *P* Value |
|---|---|---|---|
| Dynamic gain, beats·min$^{-1}$·Hz$^{-1}$ | 9.1±1.7 | 8.6±2.4 | 0.37 |
| Natural frequency, Hz | 0.062±0.014 | 0.065±0.017 | 0.10 |
| Damping ratio | 1.36±0.22 | 1.34±0.28 | 0.75 |
| Pure delay, s | 0.65±0.32 | 0.56±0.25 | 0.12 |
| Goodness of fit, % | 95.8±4.0 | 97.3±2.2 | 0.32 |
| Steady-state response, beats/min | 9.8±2.0 | 9.5±2.8 | 0.55 |
| 80% Rise time, s | 15.7±3.4 | 14.4±3.8 | 0.37 |

Data are means ± SD; $n = 7$. Exact *P* values are shown.

α-adrenergic receptors on preganglionic and/or postganglionic vagal nerve terminals to limit ACh release during vagal stimulation (24). Our observation that ANG II attenuated the dynamic gain without affecting the corner frequency or pure delay is similar to the results observed with high plasma NE, suggesting that ANG II limits ACh release during vagal stimulation. Although estimated values of the corner frequency ranged from 0.1 to 0.4 among studies, the difference may be attributable to the difference in the input signal properties (see Appendix B for details).

Although Andrews et al. (2) reported that ANG II (500 ng/kg, iv bolus) did not inhibit vagally induced bradycardia in anesthetized ferrets, Potter (31) demonstrated that ANG II (5–10 μg, iv bolus; body weight not shown) attenuated vagally induced bradycardia in anesthetized dogs. The latter study also showed that the addition of ANG II (2–5 μg/25 ml) to an organ bath attenuated vagally induced bradycardia in isolated guinea-pig atria. In that study, ANG II did not attenuate ACh-induced bradycardia, suggesting that the inhibition of bradycardia by ANG II was due to an inhibition of ACh release from vagal nerve terminals (31). In a previous study, we confirmed that intravenous ANG II (10 μg·kg$^{-1}$·h$^{-1}$) attenuated myocardial interstitial ACh release in response to vagal nerve stimulation in anesthetized cats (17). The site of this inhibitory action was thought to be parasympathetic ganglia rather than postganglionic vagal nerve terminals, because losartan, an antagonist of the ANG II receptor subtype 1 ($AT_1$ receptor), abolished the inhibitory action of ANG II when it was administered intravenously but not when it was administered locally through a dialysis fiber. ANG II may also function at the coronary endothelium and produce a diverse range of paracrine effects (6). Although the exact mechanisms remain to be elucidated, intravenous ANG II inhibits ACh release and thereby attenuates the dynamic gain of the vagal transfer function without affecting the corner frequency or pure delay.

Although the observed attenuation of the dynamic HR response to vagal stimulation by ANG II is relatively small, it may have pathophysiological significance as follows. In a previous study, our laboratory has shown that chronic intermittent vagal stimulation significantly improved the survival of chronic heart failure rats after myocardial infarction (21). In that study, the vagal stimulation intensity was such that it reduced HR only by 20 to 30 beats/min (5–10%) in rats. Therefore, change in the vagal effects on the heart, even if relatively small, could affect the evolution of heart failure. Increased plasma or tissue levels of ANG II in heart failure